Journal of Catalysis 287 (2012) 30–36

Contents lists available at SciVerse ScienceDirect

Journal of Catalysis

journal homepage: www.elsevier.com/locate/jcat

Nanostructured MnO_x as highly active catalyst for CO oxidation

Krisztina Frey [a,b,*], Viacheslav Iablokov [a], György Sáfrán [c], János Osán [d], István Sajó [e], Rafal Szukiewicz [a], Sergey Chenakin [a], Norbert Kruse [a,*]

[a] Chemical Physics of Materials, Université Libre de Bruxelles, Campus Plaine, CP243 Brussels, B-1050, Belgium
[b] Department of Surface Chemistry and Catalysis, Institute of Isotopes, Konkoly Thege Miklós út 29/33, H-1121 Budapest, Hungary
[c] Research Institute for Technical Physics and Materials Science, Konkoly Thege Miklós út 29/33, H-1121 Budapest, Hungary
[d] Atomic Energy Research Institute, Hungarian Academy of Sciences, Konkoly Thege Miklós út 29/33, H-1121 Budapest, Hungary
[e] Institute of Chemistry, Chemical Research Center, HAS, P.O. Box 17, H-1525 Budapest, Hungary

ARTICLE INFO

Article history:
Received 7 July 2011
Revised 14 November 2011
Accepted 19 November 2011
Available online 3 January 2012

Keywords:
Manganese oxide
Micro-rods and nanocrystals
XANES
XPS
CO oxidation

ABSTRACT

Non-stoichiometric Mn-oxides (MnO_x and MnO_y) were prepared by temperature-programmed oxidation (TPO) of Mn-oxalates, $MnC_2O_4{\cdot}3H_2O$ and $MnC_2O_4{\cdot}2H_2O$. Both oxides provide high specific surface areas ($525\ m^2\ g^{-1}$ and $385\ m^2\ g^{-1}$, respectively) and identical CO oxidation reaction rates of 10^{-2} molecules $nm^{-2}\ s^{-1}$ ($0.017\ \mu mol_{CO}\ m^{-2}\ s^{-1}$) at 298 K. A "spinodal" transformation of oxalates into oxides was observed by transmission electron microscopy (TEM). The quantitative evaluation of TPO and temperature-programmed reduction with CO allowed x-values of $1.61,\ldots,1.67$ to be determined for MnO_x. The Mn oxidation state in MnO_x was found to be 3.4 ± 0.1 by X-ray absorption near-edge structure analysis and X-ray photoelectron spectroscopy. In accordance with the high specific surface area and mixed-type I/IV adsorption isotherms of MnO_x, high resolution TEM demonstrated the occurrence of nested micro-rod features along with nanocrystalline particles in the endings of the rods. After CO oxidation MnO and Mn_3O_4 phases were able to be identified in the regions between rods.

1. Introduction

The oxidation of carbon monoxide (CO) is one of the "evergreens" in catalysis research. The continuing interest in this reaction is, on the one hand, sparked by environmental concerns since gaseous CO is toxic and harmful to human beings and animals. On the other hand, there are still unanswered questions of a more fundamental nature, like the low-temperature activity of certain 3d metal-oxides. While it is generally accepted that a Langmuir–Hinshelwood type mechanism (LH) between molecular CO and atomic oxygen leads to carbon dioxide (CO_2) formation on the surface of metals or metals supported by oxides, a Mars–van Krevelen type mechanism (MvK) is frequently suggested for pure metal-oxides. One of the consequences in moving from an LH to an MvK mechanism is the essential absence of CO inhibition effects for metal oxides, which is of considerable importance for achieving low-temperature activity. For example, the kinetic order dependence becomes positive in both CO and oxygen when running the reaction over spinel-type Co_3O_4 which is one of the most thoroughly studied 3d metal-oxides [1]. The high CO oxidation activity of Co_3O_4 is frequently related to the simultaneous presence of tetrahedral Co^{2+} and octahedral Co^{3+} sites [1–7]. Similarly high activity has also been reported for Mn-oxides; however, no such site requirement has ever been claimed to exist for these oxides. This is probably due to the structural flexibility of Mn-oxides which exist in a number of different stoichiometric (as MnO, Mn_2O_3, Mn_3O_4 Mn_5O_8 and MnO_2 along with their polymorphs) and non-stoichiometric phases, with the Mn valence varying smoothly between +4, as in MnO_2, and +2, as in MnO. Most of the studies on CO oxidation were performed with stoichiometric Mn-oxides. In early works, Klier and Kuchynka [8] and Kanungo [9] found high catalytic activity over bulk MnO_2 at 293 K and 353 K. Liang et al. [10] synthesized MnO_2 catalysts with nanorod morphology and found their catalytic activity to change according to $\alpha\text{-} \cong \delta\text{-} > \gamma\text{-} > \beta\text{-}MnO_2$. The variation of the catalytic activity with the polymorphism of the sample at otherwise identical bulk composition can only be explained by assuming that the specific surface termination and, consequently, the Mn–O bond strength are the determining factors. For commercially available manganese oxides the following trend of CO oxidation activity (at 523 K) has been reported by Ramesh et al. [11] and Wang et al. [12]: $MnO \leqslant MnO_2 < Mn_2O_3$. In the present study, non-stoichiometric MnO_x ($x = 1.61,\ldots,1.67$) is prepared via temperature-programmed oxidation of Mn-oxalates [13]. This oxide demonstrates even higher CO oxidation activity, with an onset far below room

---

[*] Corresponding authors. Address: Department of Surface Chemistry and Catalysis, Institute of Isotopes, Konkoly Thege Miklós út 29/33, H-1121 Budapest, Hungary (K. Frey).

E-mail addresses: frey@mail.kfki.hu (K. Frey), nkruse@ulb.ac.be (N. Kruse).

0021-9517/$ - see front matter © 2011 Published by Elsevier Inc.
doi:10.1016/j.jcat.2011.11.014

temperature. A micro-structural correlation with this activity is subsequently established and has identified MnO_x to exhibit structural features reminiscent of those of Mn_5O_8. In addition, nanocrystals are found in the endings of micro/nanorods and confer on MnO_x its unusually high specific surface area and catalytic activity. The "oxalate route" to high surface area metals and metal oxides was previously applied to produce Ni [14] and Ag on TiO_2 [15], or metal mixtures such as CoCu [16]. The present work provides the first nanostructural characterization of a highly reactive metal-oxide system prepared via oxalate precipitation.

2. Experimental section

2.1. Catalyst preparation

Catalysts were prepared in a two-step procedure. First, Mn-oxalate was precipitated from an aqueous solution of oxalic acid by adding $Mn(NO_3)_2{\cdot}4H_2O$ at room temperature while stirring continuously and adjusting the pH value to between 6 and 9 using ammonia. Precipitation was gradual with an induction period of 3–5 min. The precipitation times were 40 min and 24 h for producing $MnC_2O_4{\cdot}3H_2O$ and $MnC_2O_4{\cdot}2H_2O$, respectively, after filtration, washing and drying overnight at 343 K (see Ref. [13] for details). The as-prepared Mn-oxalates were subsequently transformed into manganese oxides using temperature-programmed oxidation (TPO) in a U-type glass reactor with a frit to deposit the sample. The decomposition/oxidation performed in a mixture of 10% oxygen in Ar with a total flow rate of 50 mL min^{-1} was followed by a quadrupole mass spectrometer (Balzers QMS 200) using a calibrated flow-through capillary while heating from room temperature to 633 K at a rate of 3 K min^{-1}. Samples were kept for 20 min at the maximum temperature before cooling them to ambient temperature in pure Ar using the same gas flow rate. In addition, for comparison purposes, a "calcined MnO_x" sample was prepared by heating $MnC_2O_4{\cdot}3H_2O$ in a crucible under the same TP conditions but using air rather than O_2/Ar.

2.2. Catalytic activities

TPO-treated samples (140 mg) were tested for their CO oxidation activity in the same apparatus. The gas flow was switched to a mixture of CO and O_2 (2% each) in Ar as vector gas using a flow rate of 50 mL min^{-1} at overall atmospheric pressure. The down-stream gas composition was analyzed mass spectrometrically. The purity of the gases was as follows: O_2 (99.995%), CO (99.997%), and Ar (99.999%). The CO conversion was calculated from the measured CO_2 formation.

2.3. Catalyst characterization

Temperature-programmed reaction studies in the presence of CO (CO-TPR) were performed to demonstrate the CO oxidation activity of MnO_x in the absence of gas phase oxygen. Manganese oxides with stoichiometric composition (Mn_2O_3 and Mn_3O_4), which can also be prepared via the oxalate route (see Ref. [13]), were subjected to the same reactivity test for comparison purposes. Samples (140 mg) were heated to 773 K in 1% CO/Ar at 3 K min^{-1} using a flow rate of 30 mL min^{-1}. The BET surface areas of manganese oxides were determined subsequent to both TPO and CO oxidation, i.e. before and after the reaction studies. The surface area measurements were performed using Ar at 77 K according to an in-situ dynamic method developed in our laboratory [17]. For comparison purposes, the MnO_x catalyst was also characterized with a TriStar 3000 instrument (Micromeritics Co.) using the N_2 adsorption/desorption method at 77 K to determine the specific surface areas as well as the pore size distribution.

XRD patterns were obtained with a Philips instrument PW 3710 equipped with a PW 1050 Bragg–Brentano parafocusing goniometer, using monochromatized Cu Kα radiation. The XRD scans were digitally recorded with steps of 0.04° in the 2θ range from 4 to 70°.

The crystal structure and morphology of the samples were investigated by using TEM. Conventional TEM analysis was performed in a PHILIPS CM20 microscope at an electron acceleration voltage of 200 kV, and HRTEM was carried out in a JEOL 3010 instrument operated at 300 kV with a resolving power of 0.17 nm. The samples for the TEM measurements were prepared by ultrasonic dispersion in distilled water and subsequent deposition of a droplet of the suspension onto a carbon-coated copper grid. The HRTEM micrographs were evaluated using Fast Fourier Transformation (FFT).

X-ray absorption near-edge structure (XANES) experiments were performed at the fluorescence beamline L of the DORIS III synchrotron ring operated by HASYLAB at the German Electron Synchrotron DESY (Hamburg, Germany). The white beam of the bending magnet was monochromatized by a Si(1 1 1) double monochromator. A polycapillary half-lens (X-ray Optical Systems, E Greenbush, NY, USA) was employed for focusing a beam of $1 \times 1\ mm^2$ down to a micrometer-sized spot (20 μm at 10 keV, 30 μm at 6.5 keV – micro-XANES mode). The absorption spectra were recorded in a fluorescence mode tuning the excitation energy near the K absorption edge of Mn (6539 eV) by stepping the Si(1 1 1) monochromator. The X-ray fluorescence photons were detected by a silicon drift detector with a 50 mm^2 active area (Radiant Vortex). The used step size varied between 0.5 (edge region) and 2 eV (more than 50 eV above the edge). The acquisition time per energy point was set to 5 s. For comparison purposes, powdered standards of pro-analysis-grade $MnCO_3$, $MnSO_4$, Mn_3O_4, MnOOH and MnO_2 with known Mn oxidation states were also investigated. In order to minimize the difference of self-absorption, microscopic grains of similar size were selected for the measurements in both the standards and the MnO_x catalyst.

X-ray photoelectron spectroscopy (XPS) measurements were performed in a combined ToF-SIMS/XPS/STM apparatus at a base pressure of 5×10^{-10} mbar using non-monochromatic Al Kα-radiation with a power of 130 W. Prior to analysis, manganese oxide samples prepared as described above were degassed in a preparation chamber (2×10^{-9} mbar) for 40 h. Photoelectron spectra were acquired with a hemispherical analyzer in the constant pass energy mode at $E_p = 50$ eV. After subtraction of the Shirley-type background the core-level spectra were decomposed into components with mixed Gaussian–Lorentzian (G/L) lines using a non-linear least-squares curve-fitting procedure. Similar to the micro-XANES studies, MnO_x was investigated along with pro-analysis-grade standard oxides MnO, Mn_3O_4, Mn_2O_3 and MnO_2. Emphasis was laid on analyzing the magnitude of the multiplet splitting of the Mn 3s photoelectron line in these samples. The carbon C 1s peak at 284.5 eV was used as reference energy for charge correction.

3. Results

As outlined in the Introduction, the thermal decomposition of Mn-oxalates in either the presence or absence of oxygen provides a convenient route to produce a variety of Mn-oxides. Crystalline and largely stoichiometric oxides as well as non-stoichiometric MnO_x are accessible in this way. According to our recent investigation, MnO_x ($x = 1.61,\ldots,1.67$) is particularly active in the catalytic CO oxidation [13]. To recall, complete CO conversion was typically obtained at room temperature or slightly below. This is shown once again in Fig. 1. In addition, to allow comparison with

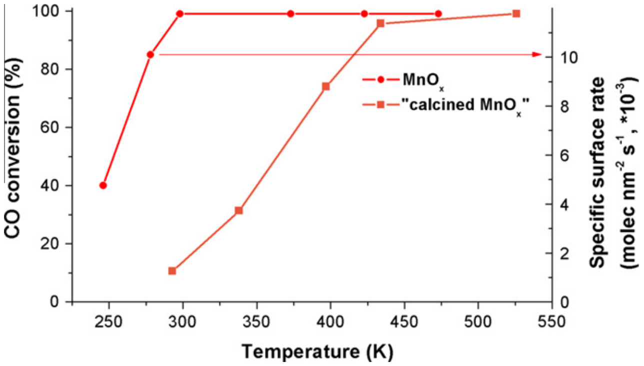

Fig. 1. Reaction rates versus time for CO oxidation (2% each, Ar as balance) over MnO_x and "calcined MnO_x" (140 mg).

literature data (for conversions below 100%), we have entered into the same figure (right-hand ordinate) the specific reaction rates as calculated from the BET data. Furthermore, we have plotted the conversion data for "calcined MnO_x" to demonstrate that the presence of water vapor during the TPO treatment causes structural and, possibly, chemical changes of MnO_x. Note that calcination did not lead to stoichiometric oxide formation; the x-value in MnO_x might have changed; however, this was not further investigated. According to the results presented in our previous investigation [13], the CO oxidation activity of "calcined MnO_x" is higher than that of stoichiometric Mn_3O_4 but lower than Mn_2O_3. The activity of MnO_x decreases gradually with time; however, the low-temperature catalytic activity can be easily recovered by a subsequent TPO treatment.

The superior catalytic activity of the MnO_x calls for a rigorous structural characterization. First TEM investigations reported in Ref. [13] have indicated that a "spinodal" decomposition of oxalate micro-rods to micro/nanorods takes place during oxidation under TPO conditions so as to produce MnO_x with a particularly high BET specific surface area of 525 $m^2\,g^{-1}$. Since Mn-oxalates are "hydrated", the first question which may be asked is if the crystallization water has a structure-directing influence on the transformation process to MnO_x during TPO. We have therefore investigated by TEM the structural features of (i) $MnC_2O_4{\cdot}2H_2O$ and $MnC_2O_4{\cdot}3H_2O$ before TPO and (ii) the oxide phases formed by TPO from these precursors under identical experimental conditions in both cases.

The TEM micrographs along with the XRD spectra of the obtained samples are presented in Fig. 2, parts a and b, respectively. According to Fig. 2a, the $MnC_2O_4{\cdot}2H_2O$ sample consists of rods about 500 nm in diameter and 3–4 μm in length together with numerous smaller broken crystals. These micro-rods are smaller than those in the $MnC_2O_4{\cdot}3H_2O$ sample which are typically about 1 μm in diameter and at least 20–30 μm in length (Fig. 2b). The XRD insets in the TEM figures (a) and (b) confirm the occurrence of crystalline $MnC_2O_4{\cdot}2H_2O$ and $MnC_2O_4{\cdot}3H_2O$, respectively. Interestingly, the rod-like structure of manganese oxalate can also be produced by a reverse-micellar method using cetyltrimethylammonium bromide as a surfactant [18].

Both oxalates were subsequently transformed into oxides using TPO (10% O_2 in Ar) under dynamic gas flow conditions so as to ensure fast removal of water and formation of XRD-amorphous/nanocrystalline structures [13]. The non-stoichiometric manganese oxides produced from $MnC_2O_4{\cdot}3H_2O$ and $MnC_2O_4{\cdot}2H_2O$ are denoted as MnO_x and MnO_y, respectively. It should be mentioned that the thermal decomposition of manganese oxalate was previously observed to lead to various forms of stoichiometric and non-stoichiometric oxides [19–21]. However, neither a structural characterization nor any catalytic properties of the resulting materials were reported in these papers.

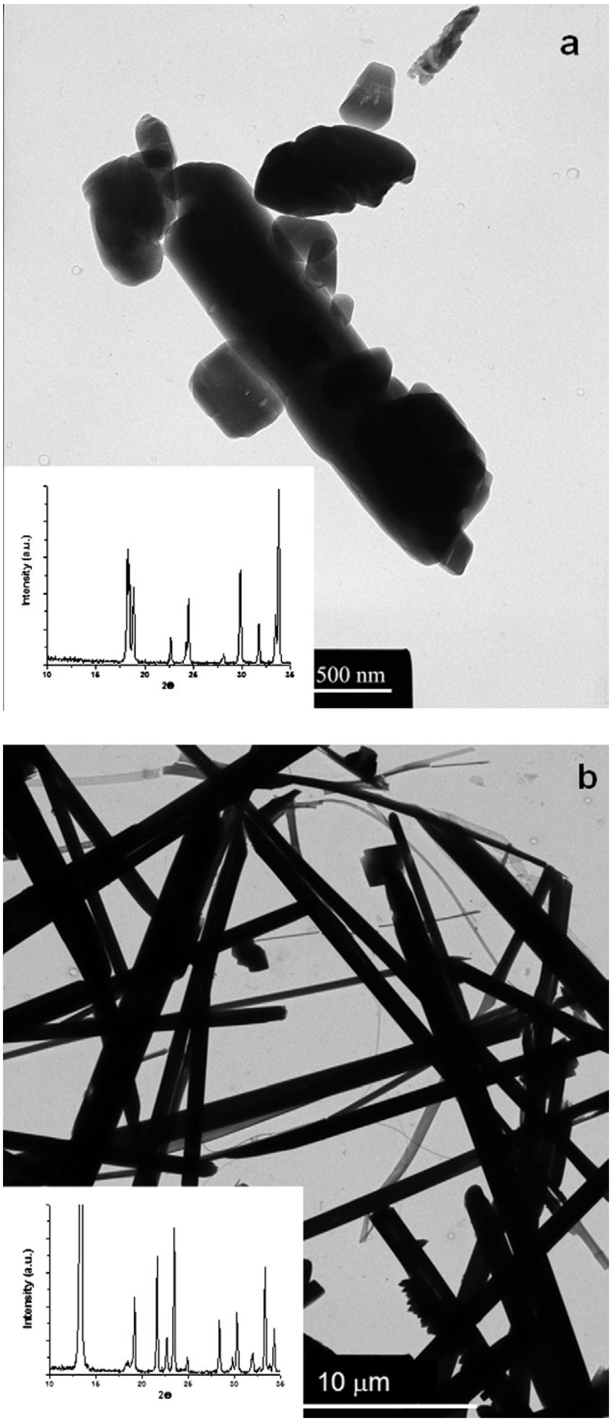

Fig. 2. Transmission Electron Microscopy images of: (a) $MnC_2O_4{\cdot}2H_2O$ and (b) $MnC_2O_4{\cdot}3H_2O$ with an inset of X-ray diffraction patterns.

In the present work, both oxides were investigated for their catalytic activity in the CO oxidation. Accordingly, MnO_x demonstrated higher activity than MnO_y if expressed in terms of $\mu mol_{CO}\,g^{-1}\,s^{-1}$. On the other hand, if the reaction rates are normalized to the BET surface areas, $S_{MnOx} = 525\ m^2\,g^{-1}$ and $S_{MnOy} = 385\ m^2\,g^{-1}$, identical rates are found. For example, at 298 K a specific reaction rate of 10^{-2} molecules $nm^{-2}\,s^{-1}$ (or 0.017 $\mu mol_{CO}\,m^{-2}\,s^{-1}$) is found for both MnO_x and MnO_y. We therefore conclude that the "spinodal" transformation of Mn-oxalate precursors with different amounts of crystallization water does not produce materials with different catalytic properties. The structural site requirements responsible for the catalytic CO oxidation are identical for both MnO_y and MnO_x. Because of the higher specific surface area, only MnO_x will be investigated in the following and compared with the properties of stoichiometric Mn-oxides.

In our previous investigation [13], arguments in favor of a Mars–van Krevelen type mechanism of CO_2 formation were provided. Accordingly, a reduction step must occur in which lattice oxygen undergoes reaction with adsorbing CO. We have therefore investigated this reaction in the absence of gaseous oxygen by ramping up the temperature in the presence of CO (CO-TPR) and comparing the behavior of MnO_x with that of Mn_2O_3 and Mn_3O_4. The results are shown in Fig. 3. Obviously, MnO_x is much more reactive than the other oxides. While CO_2 formation starts at ~300 K and extends over a broad range of temperatures up to ~700 K, both Mn_2O_3 and Mn_3O_4 react in a limited range of temperatures much higher than 300 K. The overall behavior is in agreement with a stepwise decomposition to MnO. Obviously, mixed-valence Mn_3O_4 is reduced to MnO at temperatures above 600 K, the peak maximum occurring at 713 K [22]. The reduction profile of bulk Mn_2O_3 is more complicated as two peaks with $T_{max} = 588$ K ($Mn_2O_3 \rightarrow Mn_3O_4$) and 718 K ($Mn_3O_4 \rightarrow MnO$) occur. The reduction of MnO_x shows pronounced peaks at 540 K and 683 K. The stepwise decomposition of MnO_x is a nice demonstration of the Ostwald's step rule.

In order to receive textural information, isotherms of N_2 adsorption/desorption were measured for the MnO_x sample. The results are shown in Fig. 4. Obviously, a classical type IV isotherm is obtained, with a small H4 type hysteresis loop, following the nomenclature as defined by IUPAC [23]. The occurrence of the H4 type loop is often associated with both narrow slit-like (micro-)pores and mesopores. The HRTEM results are in accordance with this conclusion, as will be shown below. Closer inspection of Fig. 4 reveals the adsorbed quantities to rise quite fast for low relative pressures ($p/p_0 < 0.1$) while the steepness at higher pressures due to multilayer adsorption is not very pronounced. Thus, while the overall behavior is typical for a type IV isotherm the influence of adsorption in micro-pores leading to a type I isotherm is clearly visible here. The occurrence of micro-pores limits the significance of pore size calculations via the Barret–Joyner–Halenda (BJH) scheme. According to Fig. 4, the distribution is characterized by a most probable pore size of 1.6 nm with 0.72 $cm^3\,g^{-1}$ pore volume. The underestimation of the pore size due to curvature effects and surface forces may reach several ten percent, however. The "*t*-plot" calculation leads to a 12% micro-pore fraction of MnO_x with a pore volume of 0.02 $cm^3\,g^{-1}$.

To provide information on the MnO_x micro-structure, TEM and HRTEM studies were performed. Our earlier TEM work has shown various morphologies comprising rods, flakes and "debris" due to the break-up of larger-size structures. In particular, nanosized features became visible at the endings of micro-rods [13]. Fig. 5 provides conventional and high resolution TEM information on the characteristic features observed after CO oxidation. Fig. 5a shows "fibrous" (rods) structures as the dominating structural feature at low magnification. Typically, such MnO_x rods are 0.1–2 μm in diameter and up to hundreds of microns in length. They are not necessarily "bulk" but rather nested; they form sheets and channels and provide a reasonable explanation for the extremely high surface area of MnO_x.

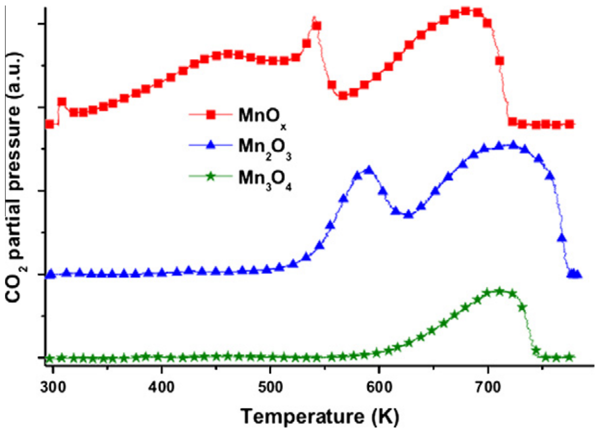

Fig. 3. CO-TPR profiles of manganese oxides.

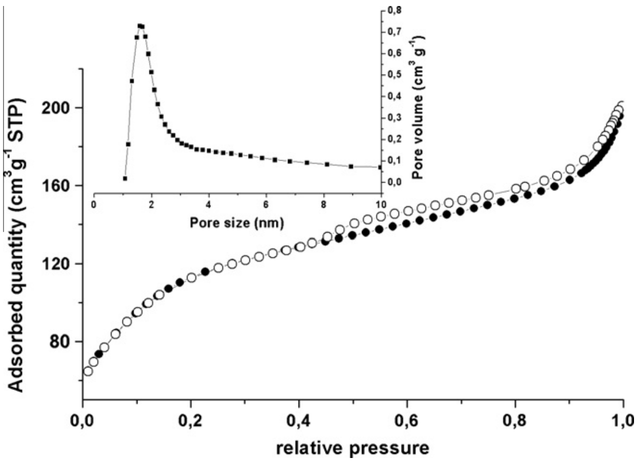

Fig. 4. N_2 adsorption/desorption isotherm for MnO_x along with *t*-plot and BJH plot.

In certain areas, the rods peel off and form flakes. The flakes typically bend and even roll up as is clearly shown in Fig. 5b. In between the rods, debris of manganese oxide appears in the form of nanocrystals 3–5 nm in size. According to HRTEM, the flakes are single crystals; their FFT patterns are identified to correspond to a tetragonal Mn_3O_4 phase (JCPDS 80-0382) (Fig. 5c). The selected area FFT of the debris shows ring patterns that correspond to the f.c.c. structure of MnO (JCPDS 75-1090) (Fig. 5d).

Flakes and debris represent only a small fraction of the entire sample. Electron transparency is limited to these structural features while rods remain virtually non-transparent so as to prevent the occurrence of sharp diffraction lines in SAED and render a chemical phase identification of MnO_x impossible. In the open endings of the rods, nanocrystalline features were detected by bright and dark field imaging as reported in our earlier investigation of the as-prepared MnO_x sample [13].

It is finally noted that fast electrons in our HRTEM analysis might cause damage to the MnO_x sample. We have seen such an influence already in our earlier work [13]. Wang et al. recently reported on a similar sensitivity when irradiating exfoliated MnO_2 sheets with electrons [24]. During their TEM measurements the (4+)-oxidation state of the manganese dioxide decreased to give way to the formation of Mn_3O_4 and MnO. Thus, electron beam irradiation caused a considerable loss in lattice oxygen. In the case of MnO_x, an increase in the size of nanocrystalline structures in between the rods (Fig. 5e and f) was observed. Possibly, the appearance of Mn_3O_4 and MnO (Fig. 5c and d) was likewise provoked by electron beam irradiation.

We finally turn to some X-ray analyses using XANES and XPS. Both techniques are element-specific and allow the chemical state of elements to be determined from the energy shifts of the absorption edge, as in XANES, or from the photoelectron lines, as in XPS. In particular, a more oxidative chemical environment of a given atom results in the shift of both the XANES absorption edge and the XPS binding energy of emitted electrons towards higher

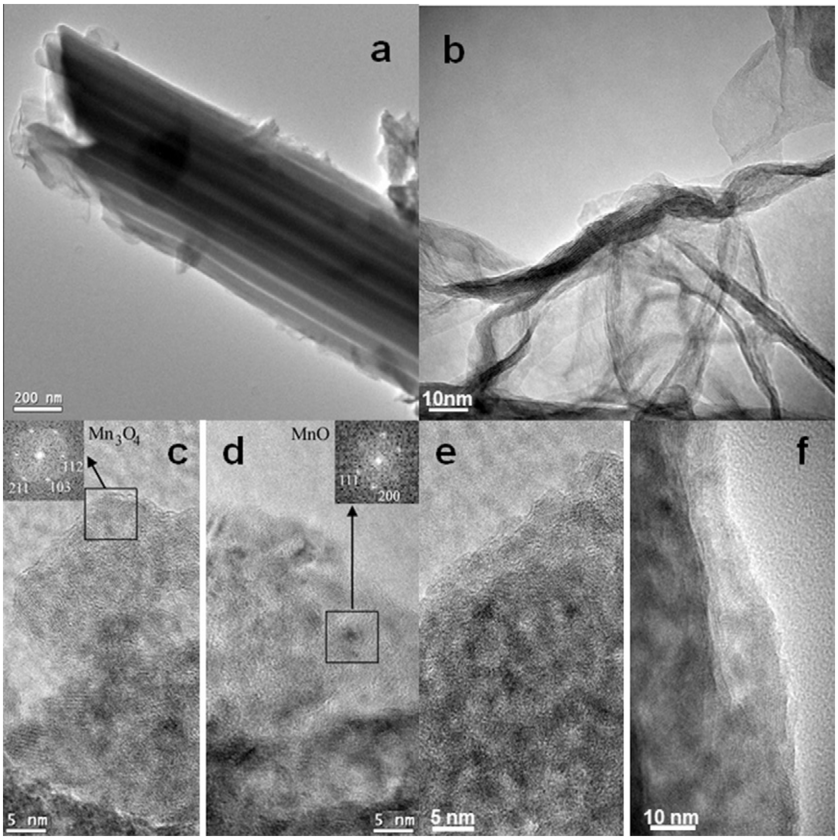

Fig. 5. Conventional and high resolution TEM micrographs of manganese oxide after TPO activation: (a) a rod, (b) a flake on the surface of a manganese oxide rod after CO oxidation at room temperature. (c) Tetragonal Mn_3O_4, (d) f.c.c. MnO phase. The Insets in (c) and (d) represent FFT-s of the areas marked by the rectangles. (e) HRTEM image taken in the first run and (f) after few minutes of exposure to electron beam.

energies. The presence or absence of pre-edge structures and the energies of near-edge structures in XANES (white line and multiple scattering resonance peaks) are also dependent on the oxidation state of the absorbing atom, but are not analyzed in the framework of the present investigation.

Fig. 6 shows the Mn K-edge micro-XANES spectra for various standard samples with different Mn oxidation states along with the spectrum from selected microscopic grains of MnO_x. The absorption edge in the MnO_x spectrum is seen to be located in between that of the MnOOH and MnO_2 standards, indicating the Mn oxidation state in MnO_x to be between 3 and 4. In order to determine the oxidation state of Mn in MnO_x, a calibration curve based on the absorption edge energies in the standards has been established. The relationship between the Mn valence state and the energy of the absorption edge has been assumed to be linear (inset of Fig. 6). The error bars represent the precision of determining the edge position and are estimated as ±0.3 eV due to the energy resolution of the monochromator (around 1 eV), the used step size (0.5 eV) and the stability of the energy scale during measurements. Taking into account the error in the edge position, the Mn oxidation state can be determined with a precision of ±0.11. The average Mn oxidation state in the MnO_x samples derived from the calibration curve is found to be 3.4 ± 0.1, which agrees well with the results of the quantitative evaluation of former TPO [13] and present CO-TPR data (see above).

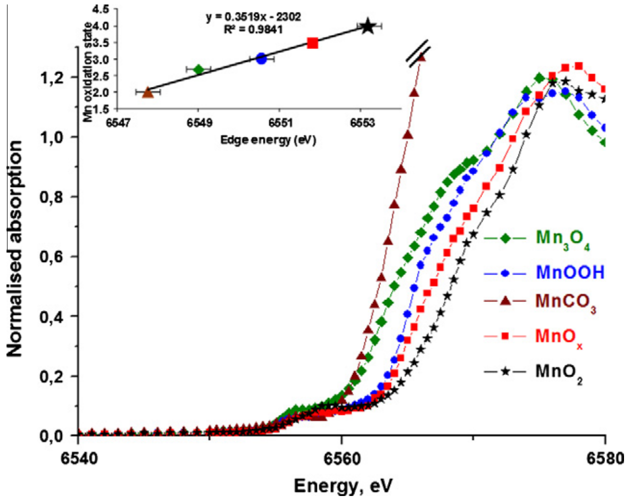

Fig. 6. Mn-K edge micro-XANES spectra of microscopic grains of standards and MnO_x with an inset of calibration line for Mn oxidation state determination based on the chemical shift of the absorption edge energy of standards.

As compared to XANES which is a bulk analysis technique, XPS provides information on metal oxidation states in layers at or close to the surface. In particular, the magnitude of the multiplet splitting of the Mn 3s photoelectron line was found [25] to noticeably vary for different Mn compounds and was therefore suggested [26] to be suitable for determining the oxidation state of Mn. We also employed this approach to evaluate the Mn oxidation state in our MnO_x catalyst. To do so, the standard oxides, MnO, Mn_3O_4, Mn_2O_3, and MnO_2, were analyzed and compared to the MnO_x catalyst. As an example, Fig. 7a shows the Mn 3s spectra for Mn_3O_4 and MnO_x on a charge-corrected binding energy scale. One can see the difference in both the energy position of the Mn 3s lines and the magnitude of multiplet splitting for the two oxides. The magnitudes of the multiplet splitting in the studied

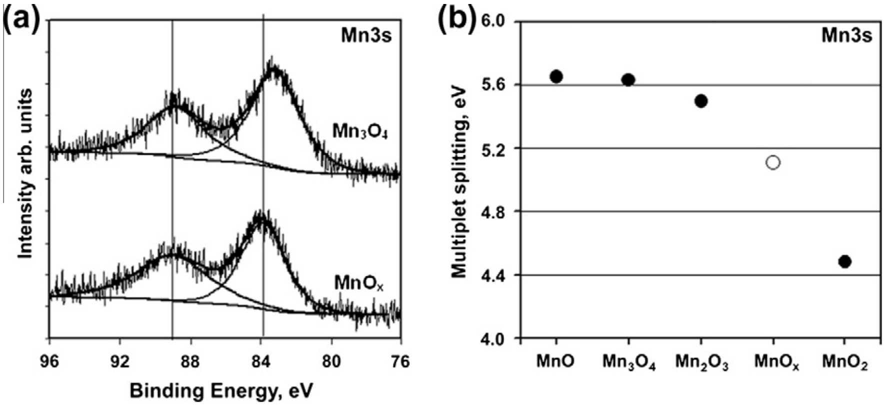

Fig. 7. (a) Mn 3s photoelectron spectra for MnO_x and Mn_3O_4, and (b) Mn 3s multiplet splitting derived from deconvolution of the Mn 3s XP spectra for MnO, Mn_3O_4, Mn_2O_3, MnO_x and MnO_2.

oxides derived from the deconvoluted Mn 3s spectra are presented in Fig. 7b. As can be seen, the multiplet energy separation decreases with an increasing Mn oxidation state, and the multiplet splitting of the MnO_x catalyst lies between that of the Mn^{3+} and Mn^{4+} states. By plotting the Mn 3s multiplet splitting versus the formal Mn valence in the oxides we evaluated the average Mn oxidation state in MnO_x. Using a linear approximation [26] for the multiplet splitting values in the oxides Mn_3O_4, Mn_2O_3 and MnO_2, a Mn oxidation state of 3.37 is finally obtained for MnO_x. Similar to the XANES bulk state analysis, this value is in very good agreement with the Mn oxidation state in MnO_x as determined by chemical titration in TPO and CO-TPR.

4. Discussion

The present paper has worked out the outstanding activity of MnO_x with respect to the catalytic CO oxidation along with a number of structural details associated with this material. The occurrence of a Mars–van Krevelen mechanism (MvK) was supported by the observation of a high susceptibility to reduction in pure CO. Interestingly, the quantitative evaluation of the CO-TPR data led to the same x-values of 1.61–1.67 for MnO_x as that of the TPO experiments published earlier [13]. Both XPS and micro-XANES allowed the Mn oxidation state in MnO_x to be determined to ~3.4 which is in good agreement with the TPO and CO-TPR titration data.

The CO oxidation reaction rate of 10^{-2} molecules $nm^{-2}\,s^{-1}$ (or 0.017 $\mu mol_{CO}\,m^{-2}\,s^{-1}$) at 298 K is lower by a factor of 10^2–10^3 as compared to supported noble metal catalysts at 523 K (see for example Ref. [1] for a comparative study of alumina-supported Pt, Pd and Rh catalysts). On the other hand, such noble metal catalysts (except for those containing nanosized Au particles [12]) are inactive at 298 K. A comparison of the activities can therefore only be made after extrapolation of the MnO_x reaction rates from 298 K to 523 K. Because of the different mechanisms of the CO oxidation over MnO_x and metal/support catalysts, this comparison must be based on turnover frequencies which need the actual site requirements to be known. To recall, while a Mars–van Krevelen type mechanism applies to MnO_x (the particularities of which are the subject of an upcoming paper), a Langmuir–Hinshelwood type mechanism applies to the above metal/support systems. The superior activity of the MnO_x catalyst as compared to stoichiometric Mn-oxides is easily demonstrated by normalizing the rates to the specific surface areas. For stoichiometric Mn_2O_3 we obtain 37 $m^{-2}\,g^{-1}$ and for Mn_3O_4 27 $m^{-2}\,g^{-1}$ leading to a reaction rate of less than 0.002 $\mu mol_{CO}\,m^{-2}\,s^{-1}$ at 298 K which is at least 10 times lower than that of MnO_x [12,13].

An intriguing feature in relation to the structural and textural properties of MnO_x is its high surface area, 525 $m^2\,g^{-1}$. A somewhat smaller value, 385 $m^2\,g^{-1}$, is found for MnO_y which was prepared by oxidation of $MnC_2O_4{\cdot}2H_2O$ precursor rather than $MnC_2O_4{\cdot}3H_2O$, as was MnO_x. However, both Mn-oxides exhibit essentially identical turnover frequencies in CO oxidation. This indicates that geometrical "defect" structures at the surface of these oxides are less important for the surface reactivity than Mn–O binding energies. A negligible structure insensitivity was also reported in studies with Co_3O_4 which is the most active among Co-oxides reported so far [1]. Xie et al. [2] and Hu et al. [3] demonstrated different CO oxidation activities on different planes of Co_3O_4 in nanorods, nanoparticles, nanobelts and nanocubes and explained this finding with the varying concentrations of Co^{3+} states in their samples.

We argued in our previous study [13] that the transformation of the Mn-oxalate is "spinodal", i.e. MnO_x inherits its morphological shape characteristics from the $MnC_2O_4{\cdot}3H_2O$ precursor which, different from $MnC_2O_4{\cdot}2H_2O$, can form mesomeric chains [27]. It is well known that the final product formation of oxalate decomposition may depend on the amount of crystallization water and on how fast this water is removed from the sample while heating. Dollimore [19] mentioned that certain oxalates, including those of manganese, may decompose in a vacuum or under low water vapor pressures to form an amorphous anhydrous material with a high surface area, while at high water pressures crystalline morphologies with a much smaller surface area are favored (Smith–Topley effect). Obviously, high water partial pressures help rearrange the structure and support recrystallization followed by growth. The influence of high water partial pressures during oxalate decomposition/oxidation is also manifest in our studies. The fast removal of crystallization water during TPO leads to the formation of MnO_x or MnO_y, while quasi-static conditions as put into effect by using air during heat treatment in a deep crucible at 633 K for 20 min produce a Mn-oxide (denoted as "calcined") whose catalytic activity in the CO oxidation is much lower than that of MnO_x or MnO_y and is between Mn_2O_3 and Mn_3O_4 [13]. A structural characterization of "calcined MnO_x" was not performed as yet and is not within the scope of the present paper.

As mentioned above, x-values between 1.61 and 1.67 corresponding to Mn oxidation states between 3.22 and 3.34 place MnO_x between Mn_5O_8 and MnO_2. There is no doubt, however, that the structural features of MnO_x are rather close to those reported for Mn_5O_8. This metastable layered Mn-oxide, exhibiting a 2:3 proportion of +2 and +4 Mn oxidation states, was reported to form in a "topotactic" conversion of γ-MnOOH nanorod precursors [28]. The details of this transformation are as little understood as those occurring in our TPO-induced transformation of Mn-oxalate to MnO_x. However, Mn_5O_8 shows well-defined large-scale crystallinity as revealed by HRTEM and electron diffraction [26] while MnO_x does not. Interestingly, during CO oxidation over MnO_x, thinner Mn_3O_4 flakes started to exfoliate from the surface so as to create petal-shaped nanosheets around the micro-rods. Also MnO was found to form in certain regions and we suspect these features are associated with the relief of strain from the MnO_x sample during CO oxidation. Petal-shaped structures are also well known for antifluorite-type MnO_2 [29,30].

Our XPS results have so far dealt with the Mn 3s multiplet splitting, because it appears to be a rather advantageous measure of the Mn oxidation state. Using binding energy of Mn 2p photoelectrons for evaluating Mn oxidation state is less reliable since, in contrast to the Mn 3s multiplet splitting, it is ambiguously influenced by charging effects. Despite this, our evaluation of the Mn 2p spectra shows that the Mn $2p_{3/2}$ binding energy for the MnO_x catalyst (641.8 eV) is noticeably larger than that for Mn_2O_3 (641.2 eV) and close to that for MnO_2 (641.9 eV). In view of the fact that the escape depth of the Mn $2p_{3/2}$ photoelectrons in MnO_2 is about 1.4 times less than that of the Mn 3s electrons, this may indicate that the Mn oxidation state in the near-surface region of the MnO_x catalyst is nearly the same as in MnO_2, but somewhat decreases in deeper layers. For more definite conclusions, a detailed analysis of the Mn 2p, Mn 3p and O 1s spectra is needed, which is currently underway.

5. Conclusion

MnO_x, MnO_y and "calcined MnO_x" have been prepared via Mn-oxalate (containing either 3 or 2 molecules of crystallization water) precipitation followed by temperature-programmed oxidation. Both MnO_x and MnO_y show nearly identical catalytic activity in the CO oxidation (10^{-2} molecules $nm^{-2}\,s^{-1}$ or 0.017 $\mu mol_{CO}\,m^{-2}\,s^{-1}$ at 298 K) when comparison is made on the basis of turnover frequencies. The MnO_x has a BET specific surface area of 525 $m^2\,g^{-1}$ and shows structural features in common with Mn_5O_8 but clearly differs from this metastable layered oxide phase by the appearance of a large amount of nanosized structures in the endings of the nano (micro-)rods. Sharp electron diffraction patterns are therefore not observed for MnO_x. However, during CO oxidation flakes start to exfoliate from the MnO_x surface so as to create petal-shaped nanosheets with local Mn_3O_4 and MnO structures between rods. Both micro-XANES and XPS confirm the oxidation state of MnO_x to be $\sim 3.4 \pm 0.1$ which is very close to that determined by titration in TPO and CO-TPR. MnO_x is prone to electron beam damage in HRTEM and X-ray damage in XPS.

Acknowledgments

V. Iablokov gratefully acknowledges PhD financial support by "ARC" (Communauté Française de Belgique) and Fond David and Alice van Buuren. K Frey has been awarded grants for short-term post-doctoral research at the ULB which are likewise acknowledged. We are also grateful to the Hungarian Science and Research Fund OTKA Grants Nos. NNF 78837, NNF2 85631 and NF-73241. The XANES measurements were carried out at the light source DORIS III at DESY, a member of the Helmholtz Association (HGF). We would like to thank Karen Appel for assistance in using beamline L. Micro-XANES studies have received funding from the European Community's Seventh Framework Programme (FP7/2007-2013) under grant agreement n° 226716.

References

[1] Yung-Fang Yu Yao, J. Catal. 33 (1974) 108–123.
[2] X. Xie, Y. Li, Z.-Q. Liu, M. Haruta, W. Shen, Nature 458 (2009) 746–749.
[3] L. Hu, K. Sun, Q. Peng, B. Xu, Y. Li, Nano Res. 3 (2010) 363–368.
[4] P. Broqvist, I. Panas, H. Persson, J. Catal. 210 (2002) 198–206.
[5] J. Jansson, J. Catal. 194 (2000) 55–60.
[6] H.-K. Lin, C.-B. Wang, H.-C. Chiu, S.-H. Chien, Catal. Lett. 86 (2003) 63–68.
[7] H.-K. Lin, H.-C. Chiu, H.-C. Tsai, S.-H. Chien, C.-B. Wang, Catal. Lett. 88 (2003) 169–174.
[8] K. Klier, K. Kuchynka, J. Catal. 6 (1966) 62–71.
[9] S.B. Kanungo, J. Catal. 58 (1979) 419–435.
[10] S. Liang, F. Teng, G. Bulgan, R. Zong, Y. Zhu, J. Phys. Chem. C 112 (2008) 5307–5315.
[11] K. Ramesh, L. Chen, F. Chen, Y. Liu, Z. Wang, Y.-F. Han, Catal. Today 131 (2008) 477–482.
[12] L.-C. Wang, Q. Liu, X.-S. Huang, Y.-M. Liu, Y. Cao, K.-N. Fan, Appl. Catal. B 88 (2009) 204–212.
[13] V. Iablokov, K. Frey, O. Geszti, N. Kruse, Catal. Lett. 134 (2010) 210–216.
[14] A. Bundhoo, J. Schweicher, A. Frennet, N. Kruse, J. Phys. Chem. C 113 (2009) 10731–10739.
[15] K. Frey, V. Iablokov, G. Melaet, L. Guczi, N. Kruse, Catal. Lett. 124 (2008) 74–79.
[16] A. Frennet, C. Hubert, E. Ghenne, V. Chitry, N. Kruse (Eds.), Proc. 12th Int. Cong. Catal.-Stud. Surf. Sci. Catal., 130, Elsevier, Amsterdam/Granada, Spain, 2000, p. 3699.
[17] A. Frennet, V. Chitry, N. Kruse, Appl. Catal. A 229 (2002) 273–281.
[18] T. Ahmad, K.V. Ramanujachary, S.E. Lofland, A.K. Ganguli, J. Mater. Chem. 14 (2004) 3406–3410.
[19] D. Dollimore, Thermochim. Acta 117 (1987) 331–363.
[20] M.I. Zaki, A.K.H. Nohman, C. Kappenstein, T.M. Wahdan, J. Mater. Chem. 5 (1995) 1081–1088.
[21] M.A. Mohamed, A.K. Galwey, S.A. Halawy, Thermochim. Acta 429 (2005) 57–72.
[22] F. Kapteijn, L. Singoredjo, A. Andreini, J.A. Moulijn, Appl. Catal. B 3 (1994) 173–189.
[23] K.S.W. Sing, D.H. Everett, R.A.W. Haul, L. Moscou, R.A. Pierotti, J. Rouquerol, T. Siemieniewska, Pure Appl. Chem. 57 (1985) 603–619.
[24] Y. Wang, C. Sun, J. Zou, L. Wang, S. Smith, G.Q. Lu, D.J.H. Cockayne, Phys. Rev. B 81 (2010) 081401. R.
[25] V.R. Galakhov, M. Demeter, S. Bartkowski, M. Neumann, N.A. Ovechkina, E.Z. Kurmaev, N.I. Lobachevskaya, Ya.M. Mukovskii, J. Mitchell, D.L. Ederer, Phys. Rev. B 65 (2002) 1131021–1131024.
[26] T. Gao, P. Norby, F. Krumeich, H. Okamoto, R. Nesper, H. Fjellvåg, J. Phys. Chem. C 114 (2010) 922–928.
[27] W.-Y. Wu, Y. Song, Y.-Z. Li, X.-Z. You, Inorg. Chem. Commun. 8 (2005) 732–736.
[28] J.H. Rask, P.R. Buseck, Am. Mineral 71 (1986) 805–814.
[29] W. Wei, X. Cui, W. Chen, D.G. Ivey, J. Power Sources 186 (2009) 543–550.
[30] W. Wei, X. Cui, W. Chen, D.G. Ivey, J. Phys. Chem. C 112 (2008) 15075–15083.